Journal of Applied Polymer Science

Influence of thermal history on crystalline morphologies of isotactic polypropylene in its miscible blends with polybutene-1

Wei Chen, Lihui Wu, Liang Chen, Zeming Qi, Liangbin Li
National Synchrotron Radiation Lab and College of Nuclear Science and Technology, CAS Key Laboratory of Soft Matter Chemistry, University of Science and Technology of China, Hefei, China
Correspondence to: L.Chen (E-mail: rychen@ustc.edu.cn) and L. Li (E-mail: lbli@ustc.edu.cn)

ABSTRACT: The miscibility behaviors in blends of isotactic polypropylene (iPP) and polybutene-1 (PB) have been studied using *in-situ* FTIR imaging. The heterogeneous melt of 3/7 iPP/PB blends were formed at 250, 220, and 180°C and then quenched to the same crystallization temperature of iPP at 125°C, respectively. Evolution processes of composition distribution during crystallization were monitored according to their characteristic peaks, and the results suggest a trend from local concentration to uniform dispersion of PB fraction. Further studies of the PB fraction as the distance from the growth front of iPP spherulite indicate an irreversible phase behavior with the progress of thermal history. The cyclic melting and crystallization favor the mixing of iPP/PB blend. Meanwhile, the nonlinear growth rate of iPP spherulite is mainly responsible for compatible promotion of iPP/PB blend, which hinders the transportation of iPP chains to its growth front. © 2015 Wiley Periodicals, Inc. J. Appl. Polym. Sci. **2016**, *133*, 43282.

KEYWORDS: copolymers; crystallization; mechanical properties; properties and characterization

Received 8 September 2015; accepted 29 November 2015
DOI: 10.1002/app.43282

INTRODUCTION

The phase behavior of polyolefin blends has been a subject of continuing interesting for researchers from both scientific and industrial fields. In general, phase transitions of crystallization and liquid-liquid phase separation are included in these blend systems. When these two nonequilibrium processes take place simultaneously, their dynamics competition might determine the final phases.[1–9] Moreover, it is well known that the difference in the melting point T_m of the two components also plays a significant role in determining the crystalline morphology.[10–13] Further studies indicate that the extent of phase segregation depends on the relation between crystallization rate of the high T_m component and the chain mobility of the low T_m component.[14–16] Meanwhile, primary nucleation of crystallization can be assisted by concentration fluctuation, especially at the interface boundaries of phase separated domains.[17–19]

Diversification of crystalline morphologies is often observed in miscible polymer blends.[20,21] Melt crystallization from a homogeneous state, crystalline component usually grows in a compact spherulitic pattern as its content is majority. In the volume-filling spherulites of high T_m component, noncrystalline of low T_m polymer is trapped in the interlamellar region, which have been confirmed by the fact that the spacing measured by small-angle X-ray scattering becomes larger as the content of the amorphous polymer increasing.[22,23] The exclusion evolution will cause the morphology changing with the distance from the center to outside of spherulite. In some cases, dendritic crystal appears at the growth front of the spherulite. While the growth rate with respect to temperature in crystalline polymer blends usually shows bell-like shape, which is nucleation limited at high temperature and diffusion limited at low temperature.[24,25] When the noncrystalline component remains trapped within interlamellar regions, spherulites continue to grow at a constant rate during crystallization. The nonlinear growth behavior is understood as the noncrystalline polymer concentrated at the growing interface which hinders the further crystal growth.

It is generally accepted that the miscibility in polymer blends must be supported by the existence of specific interactions between the components. In iPP/PB blend system, both are crystalline polyolefins which involve no specific interactions. The miscibility of iPP and PB may come from the structural similarity, which was evidenced by the depression of crystallization peak temperature and melting point temperature of each component with increasing the content of the other component.[26–29] Actually, the iPP/PB blend still experience phase separation even at 300°C, which suggests that the phase diagram can hardly be obtained by experiment. Siegmann *et al.* studied the crystallization behaviors of iPP/PB blends, which were followed by differential scanning calorimeter, and showed two separating iPP and PB crystallization processes that were both affected by the presence of each other.[30,31] Marand

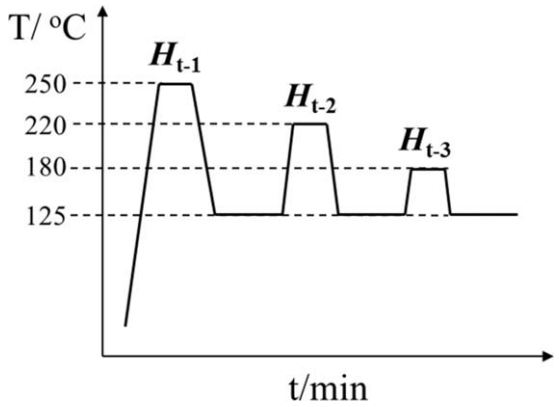

Figure 1. Thermal histories of cyclic quench conditions. The erasure time of thermal history at different temperatures is kept at 10 min.

et al. found a successively growth behavior of iPP spherulites in a phase separated liquid[32] and suggested that the iPP spherulites always nucleated in its rich phase with a compact pattern, when growth occurs within the PB-rich phase, a much more open texture is observed accompanying with a slightly decrease in growth rate.

In this work, a heterogeneous melt was chosen as an initial state to investigate the crystalline morphologies of iPP spherulite in iPP/PB blend after different thermal histories using FTIR imaging. The experimental results show that crystalline morphology and growth rate of iPP spherulite are strongly dependent on the miscibility behavior in iPP/PB blend, which may provide new sight on the dynamic progress of the correlations between the phase separation and crystallization.

EXPERIMENTAL

The iPP sample was kindly provided by SABIC-Europe with a relative weight-average molecular weight of 720 kg/mol and polydispersity of 4.8. The PB sample was purchased from Basell with a relative polydispersity of 2.8 and weight-average molecule weight of 77 kg/mol, which was determined by gel permeation chromatography. The melting temperatures of iPP and PB were about 158 and 112°C, respectively, by using a differential scanning calorimeter with heating rate of 20°C/min. The iPP/PB blends were prepared by solution precipitation method. Briefly, a desired amount of each component (with 3% weight component) was dissolved in xylene at 130°C. The hot solution was stirred over one hour and then poured into cool methanol. The white precipitates taken from the mixture were dried at room temperature and then dried under vacuum for more than 2 days at 80°C. The blend film with thickness of about 100 μm obtained by compression molding was first heated to 220°C for 10 min to erase thermal history, and then decreased to room temperature rapidly.

The experimental measurements were performed by FTIR imaging combined with a homemade hot stage with a temperature uncertainty of $\pm$0.1°C. The iPP/PB films were first put onto a ZnSe window and heated to different melting temperatures (250°C, 220°C, 180°C) for 10 min to erasure thermal history, then quenched to 125°C for isothermal crystallization. As shown in Figure 1, the melting and crystallization processes were conducted for three times in one sample. For convenience, isothermal crystallization processes after melting at 250, 220, and 180°C were termed as H_{t-1}, $H_{t-2,}$ and H_{t-3} crystallization, respectively. In order to avoid oxidation of the iPP/PB films, the progress of thermal history was performed under the protection of nitrogen atmosphere.

The isothermal crystallization processes of iPP at 125°C after melting at 250, 220, and 180°C were monitored using Bruker HYPERION 3000 microscope with FPA detector, which can acquire 4096 infrared spectra simultaneously in the region of 250×250 μm^2 with a spatial resolution of 4 μm and measuring wavenumber range of $3800 - 900$ cm^{-1}. The baselines of the spectra were carefully adjusted using the OPUS 5.5 package.

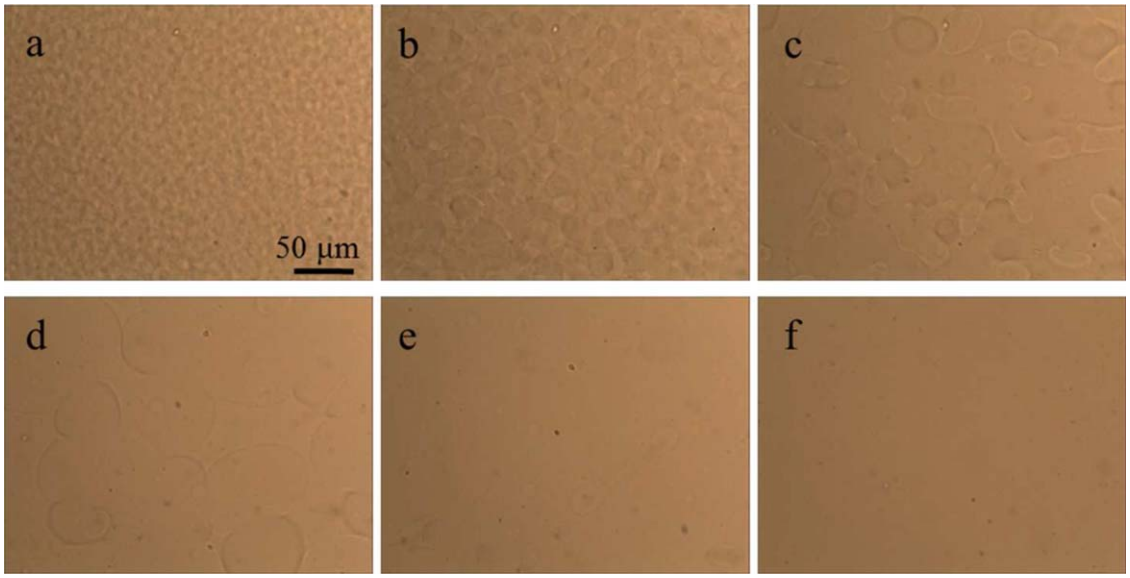

Figure 2. Optical micrographs of the 3/7 blend at 250°C for different annealing time. 1 min; (b) 2 min; (c) 4 min; (d) 6 min; (e) 8 min; (f) 10 min. [Color figure can be viewed in the online issue, which is available at wileyonlinelibrary.com.]

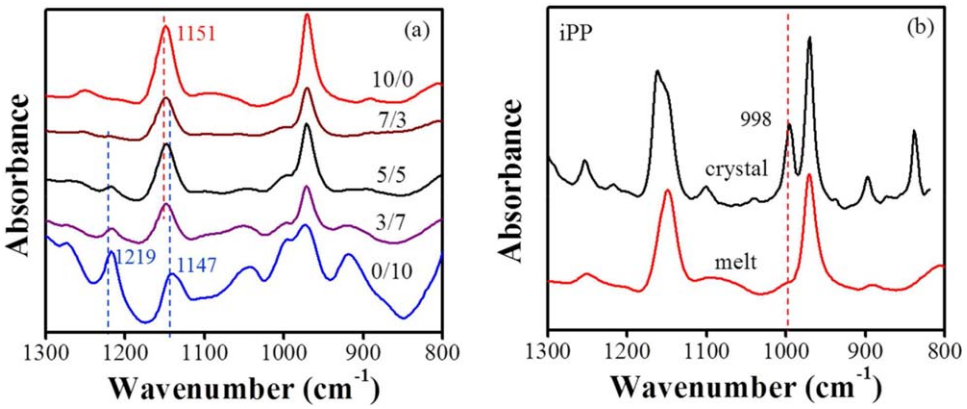

Figure 3. FTIR spectra of iPP, PB and iPP/PB blends at (a) 220°C, (b) 125°C. [Color figure can be viewed in the online issue, which is available at wileyonlinelibrary.com.]

Peak area was considered to be the integral intensity of a characteristic band in this study.

RESULTS

The optical micrographs of 3/7 iPP/PB-1 blend at 250°C as a function of annealing time are shown in Figure 2(a–f). The grainy structures observed in Figure 2(a) indicate that even after a very short residence time in liquid state, the blend is already phase separation. With longer residence times in the melt at 250°C, coarsening of the phase separation morphology can be observed more clearly [Figure 2(b,c)]. Finally the phase structure presents a homogeneous state finally [Figure 2(f)] as the blend annealed at 250°C for 10 min, the morphological evolution of interconnected domains implies that the blend undergoes a process of spinodal decomposition following by a breakup of the bicontinuous structures.

The FTIR spectra of iPP, PB and iPP/PB blends at 220°C are shown in Figure 3(a). In the spectrum of PB melt, the characteristic peaks are observed at 1219, 1147, 998, and 973 cm^{-1}, and the relative intensity of 1219 cm^{-1} to 1147 cm^{-1} remains essentially constant at 1.03, while the peaks at 1151 and 973 cm^{-1} are representative of the amorphous chains in iPP. In

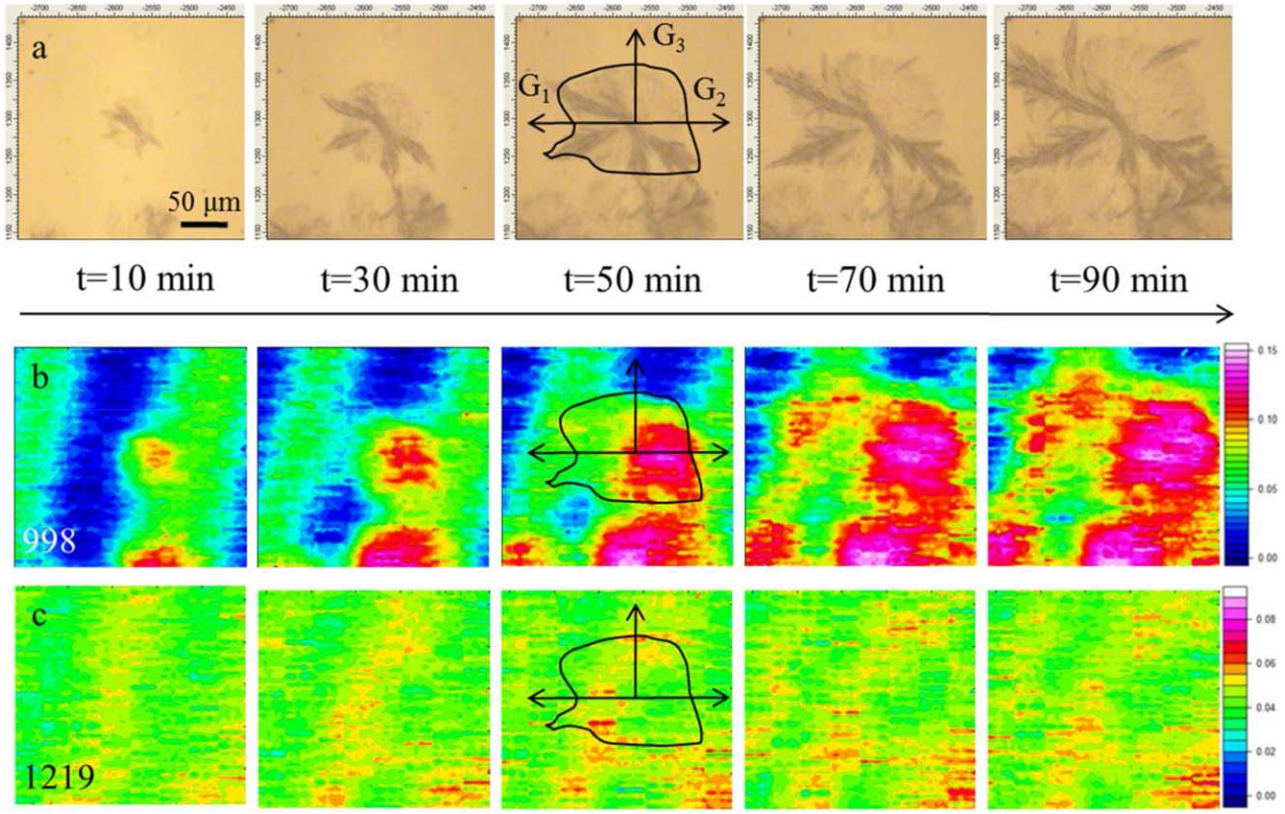

Figure 4. (a) Optical micrographs of iPP spherulite in 3/7 blend crystallized at 125°C for various crystallization times after melting at 250°C for 10 min. Images of infrared absorbance at 998 cm^{-1} (b) and 1219 cm^{-1} (c). [Color figure can be viewed in the online issue, which is available at wileyonlinelibrary.com.]

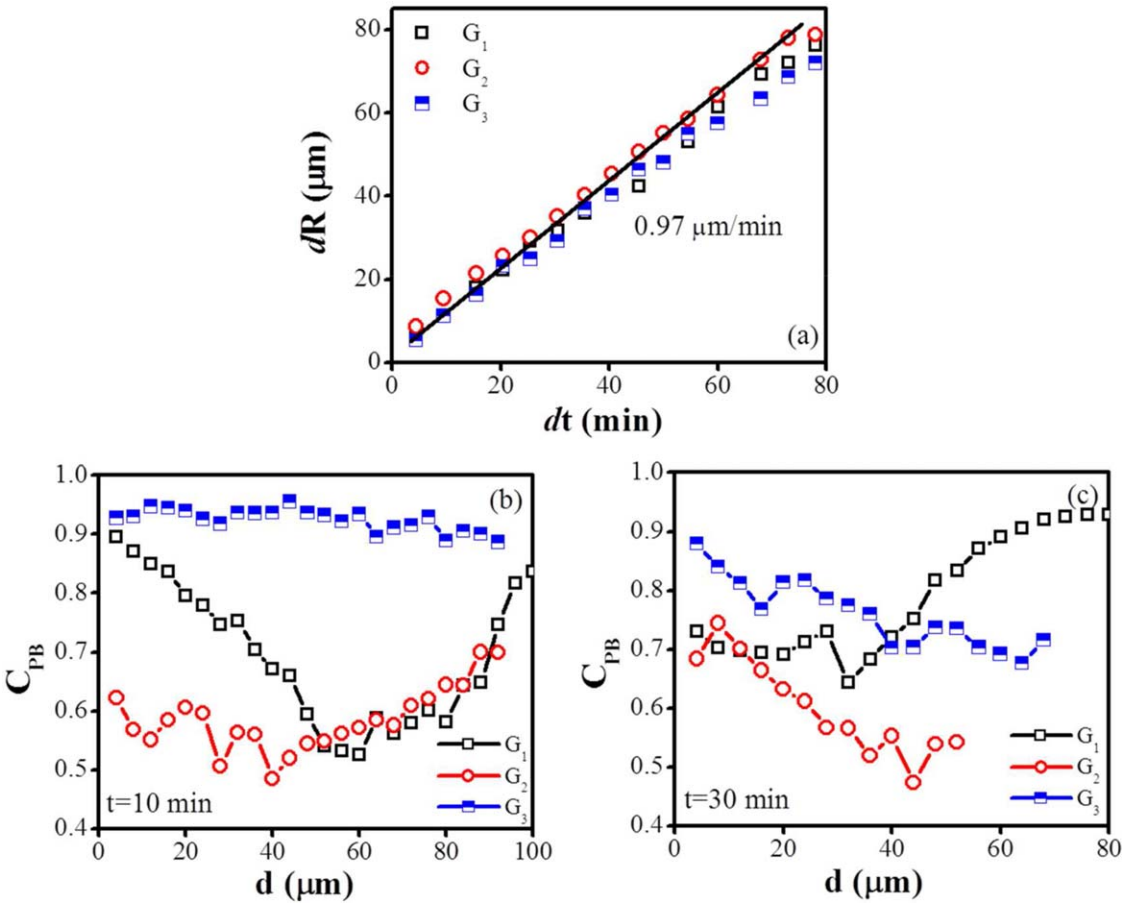

Figure 5. (a) Variations of spherulite radius of iPP in 3/7 blend during H_{t-1} crystallization at different growth directions. Composition profiles of PB as a function of the distance from the growth front of the iPP spherulite at various crystallization times (b) 10 min, (c) 30 min. [Color figure can be viewed in the online issue, which is available at wileyonlinelibrary.com.]

blends with different composition at 220°C, the peak located at 1151 cm^{-1} are formed through the overlapping between 1151 cm^{-1} of iPP and 1147 cm^{-1} of PB. Thus, the PB fraction at the growth front of the iPP spherulite in the blend can be determined by the independent of 1219 cm^{-1} using eq. (1) because the corresponding peak of iPP emerges only in crystals [see Figure 3(b)].[33,34]

$$C_{PB} = \frac{A_{1219}}{A_{1219} + kA_{1151}} \quad (1)$$

Figure 4(a) shows the optical micrographs of iPP spherulite in 3/7 blend at 125°C after melting at 250°C for 10 min. A loosing spherulite with part of highly branched morphology is obtained. The same area of iPP- and PB-specific FTIR images of the 3/7 blend are presented in Figure 4(b,c). The value of each pixel is expressed as a color bar at the right side, where red zone represents a high concentration of the respective composition, while the blue represents the composition with low component.[35] The results indicate that even quenched from 250°C, the 3/7 blend experience phase separation. Interestingly, there is a mismatching between the images of infrared absorbance at 998 cm^{-1} and the spherulite contour as marked in black solid lines. In the region of spherulite, the area of weak absorption is corresponding to the PB-rich phase at the beginning of crystallization, which indicates that PB droplets are gathering into a larger domain size in iPP spherulites. It is clear that the PB-rich phase is trapped within the growing spherulites.

In order to analyze the influence of PB distribution on the growth behavior of composition, variations of spherulite radius of iPP at different growth directions (as depicted in Figure 4) during H_{t-1} crystallization are summarized in Figure 5(a). Linear crystal growth rates with identical slope are observed in the whole analyzed directions range up to spherulite impingement, which indicate the hindrance of crystallization by PB concentration is not obvious. As a consequence, the iPP spherulite can reach larger dimension without being confined. The composition profiles C_{PB} as the distance from the growth front of the iPP spherulite in corresponding directions are shown in Figure 5(b,c), respectively. A significant fluctuation of the PB fraction from 0.4 to 1.0 has been observed at the early stages of crystallization ($t = 10$ min). The composition profiles at the growth front will change with time and develop in the surroundings.

The dependence of crystalline morphologies on thermal history was further investigated. Figure 6(a) shows the H_{t-2} crystallization process at 125°C. Note that no structures of phase separated can be observed in microscopy above melting temperature of iPP crystals. In comparison with H_{t-1}, there is no obvious

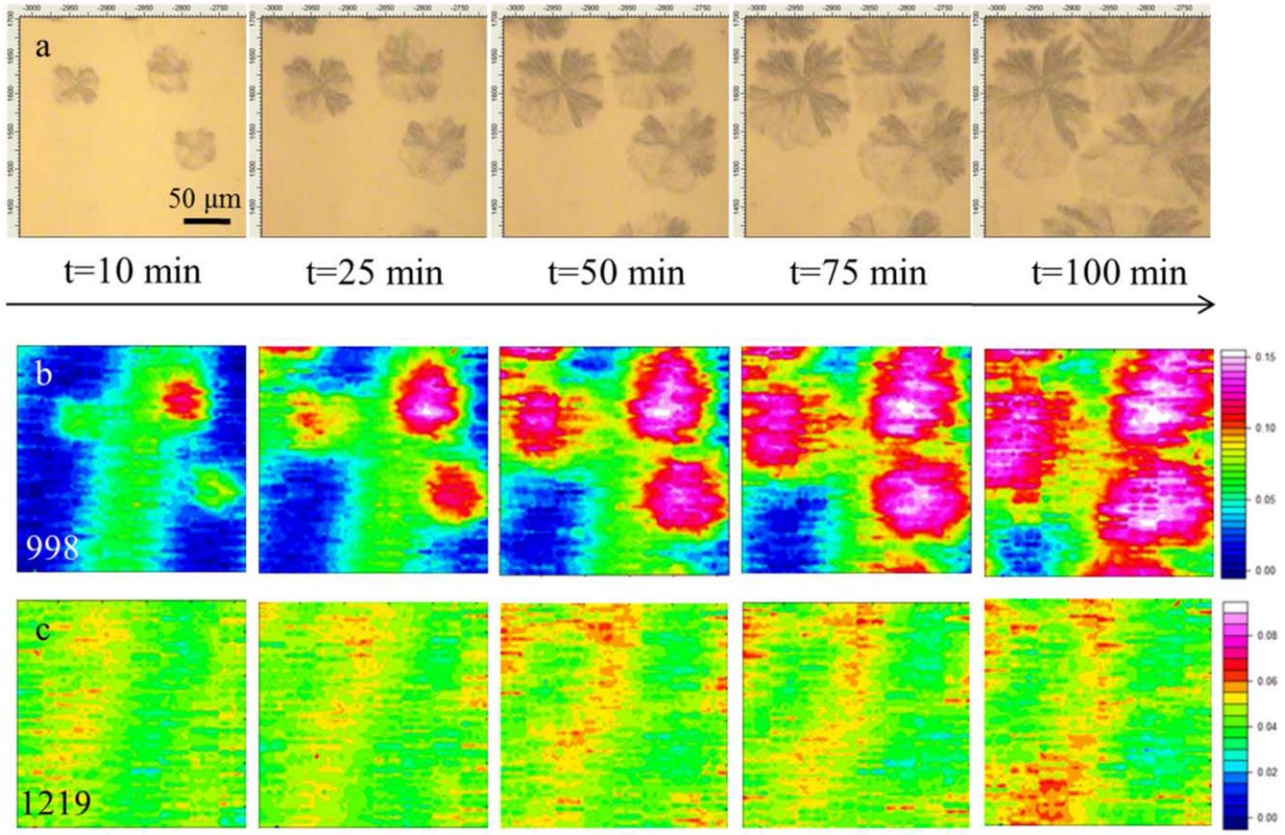

Figure 6. (a) Optical micrographs of iPP spherulite in 3/7 blend crystallized at 125°C for various crystallization times after melting at 220°C for 10 min. Images of infrared absorbance at 998 cm^{-1} (b) and 1219 cm^{-1} (c). [Color figure can be viewed in the online issue, which is available at wileyonlinelibrary.com.]

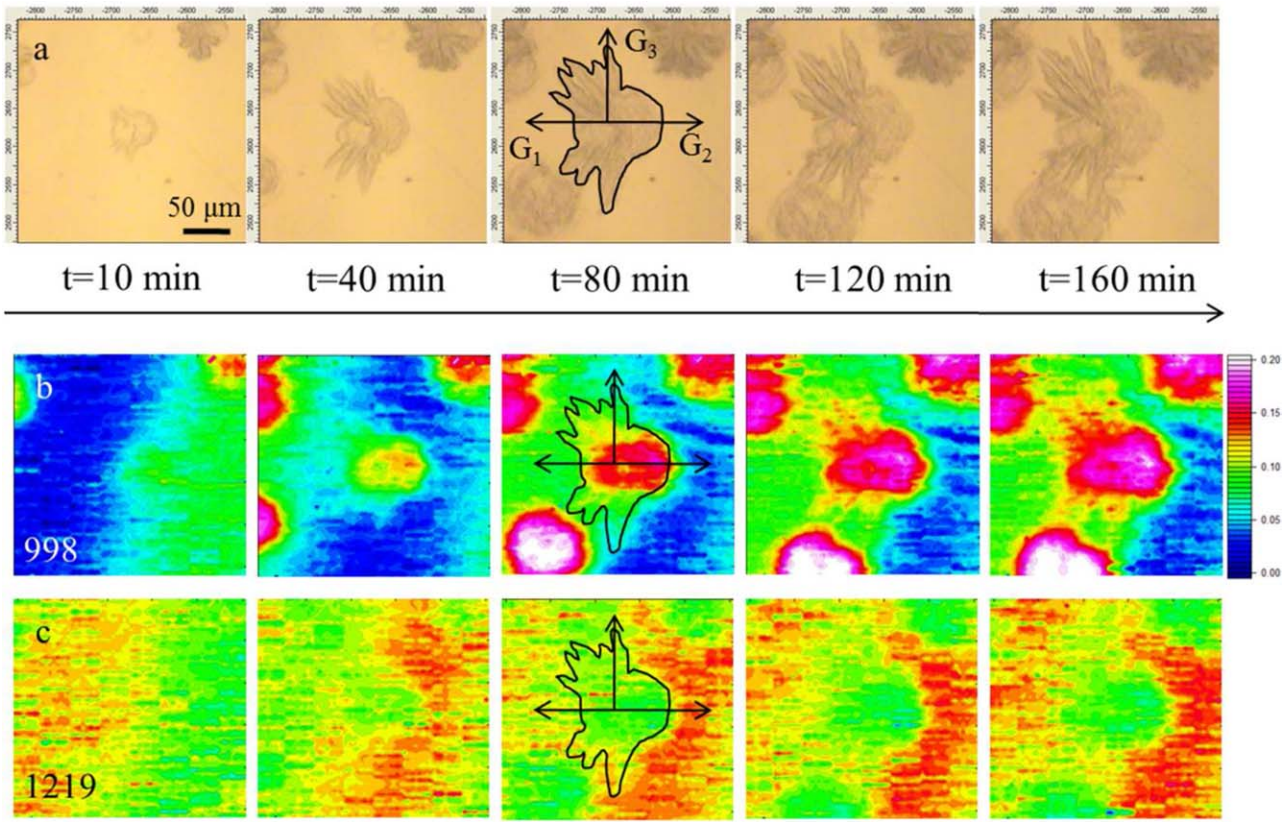

Figure 7. (a) Optical micrographs of iPP spherulite in 3/7 blend crystallized at 125°C for various crystallization times after melting at 180°C for 10 min. Images of infrared absorbance at 998 cm^{-1} (b) and 1219 cm^{-1} (c). [Color figure can be viewed in the online issue, which is available at wileyonlinelibrary.com.]

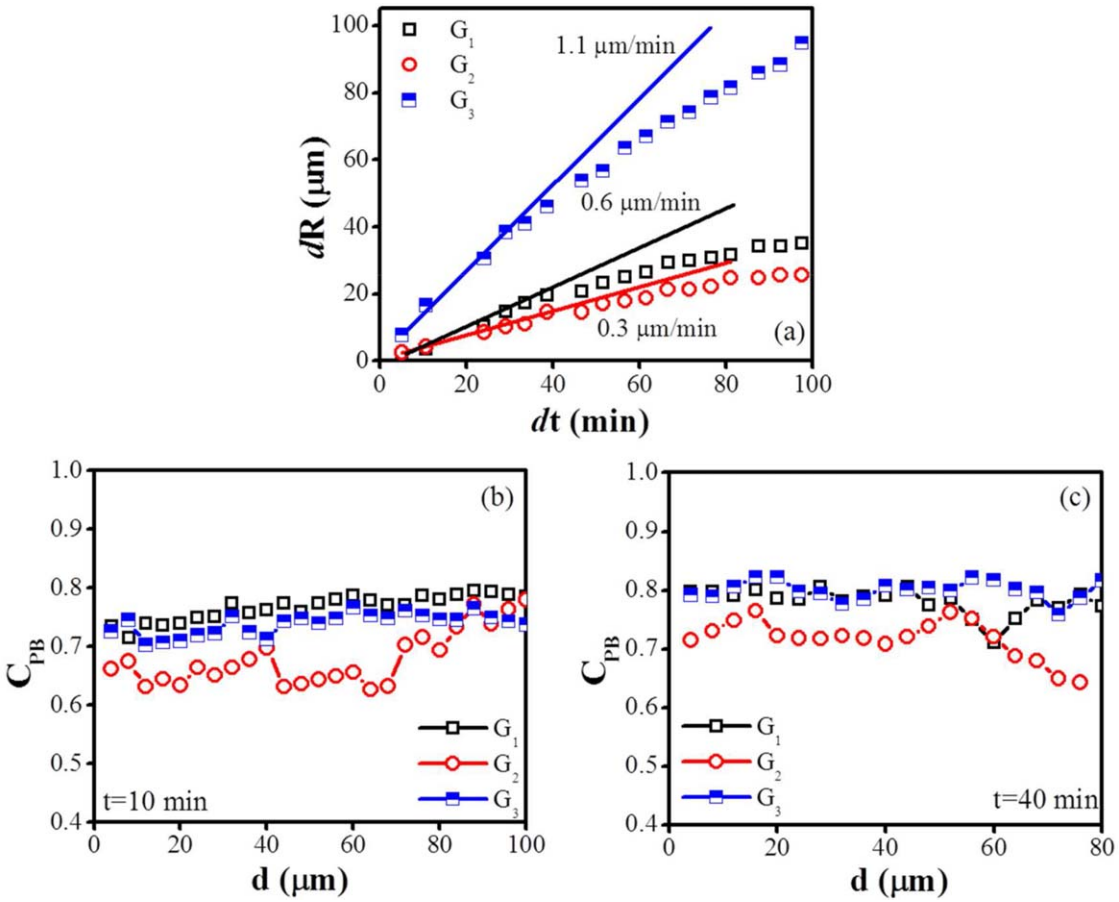

Figure 8. (a) Variations of spherulite radius of iPP in 3/7 blend during H_{t-3} crystallization at different growth directions. Composition profile of PB as a function of the distance from the growth front of the iPP spherulite at various crystallization times (b) 10 min, (c) 40 min. [Color figure can be viewed in the online issue, which is available at wileyonlinelibrary.com.]

change of crystalline morphology during the H_{t-2} crystallization. In the FTIR images [Figure 6(b,c)], iPP- and PB-rich phases can be clearly distinguished. The spherulitic regions correlate with the red areas of the iPP image and the green areas of the PB image very well, suggesting a trend from local concentration to uniform dispersion of PB fraction, while composition heterogeneity also exist during the initial stages of crystallization.

After completion of crystallization, the blend was heated to 180°C for 10 min, and the subsequent H_{t-3} crystallization process is presented in Figure 7(a). It can be seen that the iPP spherulite exhibits a significant change by showing diversification into multiple spherulite patterns. Growth rate of flower-like spherulites start to slow down until the size reaches about 100 μm. Meanwhile, new structure of dendritic morphology appears at the growth front of the spherulite. In addition, isothermal crystallization does not reach completion at 125°C, as the growth front stops before impingement occurs. Figure 7(b,c) present good correspondence to the composition distribution. With the progress of heat treatments, an irreversible phase behavior leads to different segregations of two components in the melt.

In Figure 8(a), the results from evaluation of the spherulite growth rate are also summarized in corresponding directions during H_{t-3} crystallization. Nonlinear growth behavior of iPP spherulite occurs after erasure of thermal history for three times. Spherulite radius increases linearly with time at first and then decreases at later stages, which is attributed to the hindrance of crystallization by PB component at the growth front of the iPP spherulite. Compared with the H_{t-1}, growth rate becomes lower during H_{t-3} crystallization. In Figure 8(b,c), the fluctuation of PB fraction around iPP spherulite decreases. Changes of C_{PB} are close to the original composition at 0.7. This indicate thermal history promote compatible instead of phase separation.

DISCUSSION

In this study, heterogeneous melt of iPP/PB blend was used as the initial state to study the influence of thermal history on the crystallization behaviors of iPP. Two important conclusions can be drawn. First, cyclic melting and crystallization favor the mixing of iPP/PB blend. This can be understood by the changes of composition profiles around the spherulite. Local concentration of PB fraction reflects narrow distribution of characteristic wavelength developed by the first melting and the subsequent crystallization. In the following process of thermal history, C_{PB} fluctuation decreases, causing a broaden periodicity distribution. This may be a possible reason explaining why the phase

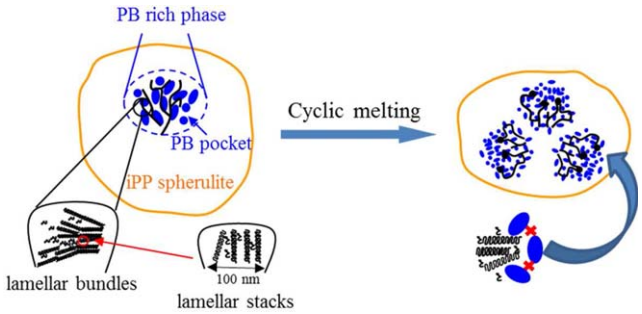

Figure 9. Schematic diagram of the phase behavior during cyclic melting and crystallization. [Color figure can be viewed in the online issue, which is available at wileyonlinelibrary.com.]

separated structure is difficult to observe after removal of thermal history at the first time.

The second conclusion is that, the growth rate of iPP spherulite is mainly responsible for the effect of thermal history. For the composition with the same conditions, the growth rates decrease gradually and deviate from the linear growth with the progress of thermal history. It is should be pointed out that the growth behavior mentioned above always exists whether erasure thermal history from high melting temperature or low melting temperature. This indicates that evolution of phase structure is the mechanism behind the dependence of the growth rate on the thermal history rather than undercooling effect of equilibrium melting-point depression. The spherulite growth rate in polymer blends is mainly related to the transport capacity of chains to the growth front. Competition between crystallization and diffusion chain displacement were usually proposed to explain the self-decelerated crystallization associated with the nonlinear growth behavior. The exclusion of low-T_m component can be controlled by the crystallization temperature and the diffusion rate increases uniformly with temperature. In contrast, the growth rate exhibits a maximum between the glass-transition temperature and the equilibrium melting temperature. In terms of the diffusion-controlled growth of spherulites, the increase in the concentration of the low-T_m component at the growth front will induce the nonlinear growth behavior.

However, cyclic quench experiments were carried out at the same crystallization temperature. It means that the diffusion of the amorphous chains has almost the same mobility during crystallization. Therefore, the origin of the decreased growth rate could be ascribed to the promotion of compatibility in iPP/PB blend. A schematic is presented in Figure 9 to show the effect of phase structures on their subsequent crystallization. The bundles of lamellar stacks formed at the local concentration of PB fraction are irregularly arranged. Because of amorphous pockets on a micrometer scale beyond the scale of the interlamellar spacing, it may be expected that the growing interface easily keeps away from the areas of PB pocket. With the proceeding of melting and crystallization, the amorphous pockets become smaller than that to the same size with the lamellae stacks. The "homogenous distribution" of PB component hinders thecrystallization and causes a decrease in the growth rate of spherulite.

CONCLUSIONS

In this study, miscibility behaviors in blends of iPP and PB undergoing three different thermal histories are investigated using *in situ* FTIR imaging. The results indicate that cyclic melting and crystallization promote the mixing of two components in iPP/PB blend. During the first crystallization, there is a mismatching between the iPP-specific FTIR images and the spherulite contour. It is clearly that the PB-rich phase is trapped within the growing spherulites. After completion of H_{t-1} crystallization, it is found that a trend from local concentration to uniform dispersion of PB fraction in the subsequent H_{t-2} and H_{t-3}crystallization processes. Changes of C_{PB} profile around the spherulite are close to the original composition at 0.7. Moreover, the heterogeneous melt always exist before crystallization. The results also indicate the new structure of dendritic morphology appears at the growth front of the spherulite with the progress of thermal history accompanying with the growth rates decreasing, which can be attributed to hindrance of crystallization by homodisperse PB component in blend.

REFERENCES

1. Yao, Y.; Dong, X.; Zhang, C.; Zou, F.; Han, C. C. *Polymer* **2010**, *51*, 3225.
2. Shimizu, K.; Wang, H.; Matsuba, G.; Wang, Z.; Kim, H.; Peng, W.; Han, C. C. *Polymer* **2007**, *48*, 4226.
3. Jin, J.; Chen, H.; Muthukumar, M.; Han, C. C. *Polymer* **2013**, *54*, 4010.
4. Zhang, X.; Wang, Z.; Zhang, R.; Han, C. C. *Macromolecules* **2006**, *39*, 9285.
5. Wang, T.; Li, H.; Wang, F.; Yan, S.; Schultz, J. M. **2011**, *115*, 7814.
6. Wang, T.; Li, H.; Wang, F.; Schultz, J. M.; Yan, S. *Polym. Chem.* **2011**, *2*, 1688.
7. Penning, J. P.; Manley, R. S. J. *Macromolecules* **1996**, *29*, 77.
8. Penning, J. P.; Manley, R. S. J. *Macromolecules* **1996**, *29*, 84.
9. Dong, L. S.; Olley, R. H.; Bassett, D. C. *J. Mater. Sci.* **1998**, *33*, 4043.
10. Qiu, Z. B.; Ikehara, T.; Nishi, T. *Polymer* **2003**, *44*, 2799.
11. Qiu, Z. B.; Ikehara, T.; Nishi, T. *Macromolecules* **2002**, *35*, 8251.
12. Qiu, Z. B.; Fujinami, S.; Komura, M.; Nakajima, K.; Ikehara, T.; Nishi, T. *Polymer* **2004**, *45*, 4355.
13. Qiu, Z.; Yan, C.; Lu, J.; Yang, W. *Macromolecules* **2007**, *40*, 5047.
14. Zheng, S.; Jungnickel, B. J. *J. Polym. Sci. Part B-Polym. Phys.* **2000**, *38*, 1250.
15. Liu, J. P.; Jungnickel, B. J. *J. Polym. Sci. Part B-Polym. Phys.* **2006**, *44*, 338.
16. Kalivianakis, P.; Jungnickel, B. J. *J. Polym. Sci. Part B-Polym. Phys.* **1998**, *36*, 2923.
17. Shi, W.; Yang, J.; Zhang, Y.; Luo, J.; Liang, Y.; Han, C. C. *Macromolecules* **2012**, *45*, 941.
18. Shi, W.; Xie, X. -M.; Han, C. C. *Macromolecules* **2012**, *45*, 8336.

19. Shi, W.; Han, C. C. *Macromolecules* **2012**, *45*, 336.
20. Ni'mah, H.; Woo, E. M.; Nurkhamidah, S. *J. Polym. Res.* **2013**, *21*,
21. Okabe, Y.; Murakami, H.; Osaka, N.; Saito, H.; Inoue, T. *Polymer* **2010**, *51*, 1494.
22. Tanaka, H.; Nishi, T. *Phys. Rev. Lett.* **1985**, *55*, 1102.
23. Hudson, S. D.; Davis, D. D.; Lovinger, A. J. *Macromolecules* **1992**, *25*, 1759.
24. D.; Lorenzo, M. L.; Righetti, M. C. *J. Polym. Sci. Part B-Polym. Phys.* **2007**, *45*, 3148.
25. Di Lorenzo, M. L. *Prog. Polym. Sci.* **2003**, *28*, 663.
26. Ardakani, F.; Jahani, Y.; Morshedian, J. *J. Appl. Polym. Sci.* **2012**, *125*, 640.
27. Hsu, C. C.; Geil, P. H. *Polym. Eng. Sci.* **1987**, *27*, 1542.
28. Shieh, Y. T.; Lee, M. S.; Chen, S. A. *J. Polym. Sci. Part B-Polym. Phys.* **2002**, *40*, 638.
29. Shieh, Y. T.; Lee, M. S.; Chen, S. A. *Polymer* **2001**, *42*, 4439.
30. Siegmann, A. *J. Appl. Polym. Sci.* **1982**, *27*, 1053.
31. Siegmann, A. *J. Appl. Polym. Sci.* **1979**, *24*, 2333.
32. Cham, P. M.; Lee, T. H.; Marand, H. *Macromolecules* **1994**, *27*, 4263.
33. Lee, J. Y.; Painter, P. C.; Coleman, M. M. *Macromolecules* **1988**, *21*, 954.
34. Lee, J. Y.; Painter, P. C.; Coleman, M. M. *Macromolecules* **1988**, *21*, 346.
35. Vogel, C.; Wessel, E.; Siesler, H. W. *Macromolecules* **2008**, *41*, 2975.